Proton-loaded zeolites. 1. HX (X = Cl, Br, I) in sodium zeolite Y archetype: Packaged acids on the road to intrazeolite semiconductors

ARTICLE *in* CHEMINFORM · APRIL 1990

Impact Factor: 0.74 · DOI: 10.1021/j100382a047

3 AUTHORS, INCLUDING:

Saim Özkar
Middle East Technical University
298 PUBLICATIONS **5,295** CITATIONS

Proton-Loaded Zeolites. 1. HX (X = Cl, Br, I) in Sodium Zeolite Y Archetype: Packaged Acids on the Road to Intrazeolite Semiconductors

Geoffrey A. Ozin,* Saim Özkar,† and Galen D. Stucky‡

Lash Miller Chemistry Department, University of Toronto, 80 St. George Street, Toronto, Ontario, Canada M5S 1A1 *(Received: January 12, 1990; In Final Form: April 4, 1990)*

This series of three papers is concerned with an in-depth investigation of proton-loaded zeolites (packaged acids), a novel class of controlled microporosity, solid-state Brønsted acids. Proton-loaded zeolites are formed from the reaction between anhydrous Brønsted acids and dehydrated zeolites. Initial experiments focus attention on the chemistry, spectroscopy, diffraction, and dynamics of the sorption and desorption of anhydrous hydrogen halides (HX) in zeolite Y with some important control experiments in all-silica zeolite Y (SiO_2-Y) and ALPO-5. Zeolite cation, HX anion, H/D isotope, and probe-base effects are explored to elucidate details of location, population, distribution (homogeneity), thermal/kinetic stability, acidity, and reactivity of protonation, anionation, and sólvation sites in the zeolite Y lattice. Studies designed to probe the OH bond strength, acidity, solvation, and H/D isotope-exchange characteristics of proton-loaded zeolite Y leave little doubt that protonated oxygen framework sites and Brønsted acid sites in zeolite Y are for most purposes "identical". This study also alerts one to the fact that the types of adsorption, ionization, charge separation, and solvation phenomena that ensue following the sorption of anhydrous HX into zeolite Y have an important bearing on the designed synthesis of monodispersed intrazeolite semiconductor halide, sulfide, and phosphide quantum dots, wires, and supralattices that can be formed from similar kinds of acid–base reactions between anhydrous HX, H_2S, and PH_3, and extraframework cations in zeolite Y. The first part of this study focuses attention on the sodium zeolite Y system, which is considered as the archetypical model for the proton-loaded zeolite. This is followed in the second part with investigations relating to acidity, cation, and dehydrohalogenation effects of proton-loaded zeolites and how they compare with normal Brønsted acid zeolites and their decationization properties. The last part of this study enquires into the protonation of Brønsted acid zeolite Y, as well as the cation-free dipolar hydrophilic lattice of ALPO-5 and the hydrophobic lattice of SiO_2-Y.

Introduction

The tremendous current interest in semiconductor ultramicrostructures can be considered to derive from the original notion of artificially layered structures known as semiconductor superlattices and from the exciting optical and electrical properties that such quasi-two-dimensional (2D) electron systems offer.[1] A major challenge in the synthesis of spatially resolved materials is the reproducible fabrication of microscopically organized, monodisperse semiconducting solids having quasi-1D and quasi-0D electronic/optical properties. Strongly enhanced electron mobilities, resonant tunneling quantum effects, and optical nonlinearities have been predicted and recently observed in the case of quantum wires (1D) and quantum boxes (0D).[2]

In semiconductor physics, such 1D and 0D quantum microstructures are usually accessed through molecular beam epitaxy (MBE) and metal organic chemical vapor deposition (MOCVD, planar engineering) coupled with electron beam lithography (EBL) and reactive ion-etching (RIE, lateral engineering) techniques.[2] These methods are instrumentally sophisticated and very costly. Also they have minimum size and dispersion limitations of around 100 ± 30 Å. As a way to circumvent these difficulties, quantum size particles have been prepared and studied in various host matrices including glasses, micelles, vesicles, ionomers, Langmuir–Blodgett (LB) films, clays, felspathoids, and zeolites.[3] Topotactic chemical approaches involving zeolites have a distinct advantage over the other matrices commonly employed because they permit the controlled growth and ordered inclusion of semiconductor particles with very small dimensions and very uniform size distribution.[3,4]

Metal chalcogenides currently represent the class of most well studied intrazeolite semiconductor quantum objects.[3,4] Lattice fillers such as CdS, PbS, and CdSe are usually introduced into the zeolite via the topotactic reaction of extraframework Cd^{2+} or Pb^{2+} with gaseous H_2S or H_2Se. Clearly, whatever the detailed mechanism of this process, the requirement of overall charge balance between the oxygen framework and extraframework cations necessitates that the embibed semiconductor particles be born and housed in a Brønsted acid environment. If one is to control the nucleation, growth, stabilization, and location of intrazeolite semiconductor clusters using the above kind of acid–base chemistry, it is important to try to gain an understanding of the details of the process and what factors control the individual events that lead up to the encapsulation, immobilization, and positioning of the semiconductor guest.

At this point it is pertinent to recognize the relationship of the aforementioned H_2S/MZ experiments to some early work of Barrer and co-workers[5] concerning the adsorption of anhydrous hydrogen halides HX (where X = Cl, Br, I) into different zeolite types. Barrer's 1970 ideas can be represented with the chemical equilibria

$$\mathrm{MOZ} + n\mathrm{HX(g)} \rightleftarrows n(\mathrm{HX})_a\mathrm{MOZ} \rightleftarrows (n-m)(\mathrm{HX})_a m(\mathrm{MX})_{o,i}\mathrm{M}_{1-m}\mathrm{H}_m\mathrm{OZ}$$

† On leave of absence from the Chemistry Department, Middle East Technical University, Ankara, Turkey.

‡ Department of Chemistry, UCSB, Santa Barbara, CA 93106.

(1) Narayanamurti, V. *Science* **1987**, *235*, 1023. Ploog, K. *Angew. Chem., Int. Ed. Engl.* **1988**, *100*, 611, and references therein.

(2) Randall, J. N.; Reed, T. M.; Moore, R. T.; Matyi, J. W.; Lee, J. *J. Vac. Sci. Technol.* **1988**, *B6*, 302. Tsuchiya, M.; Gaines, J. M.; Yan, R. H.; Sinies, R. J.; Holtz, P. O.; Coldren, L. A.; Petroff, P. M. *Phys. Rev. Lett.* **1989**, 466. Reed, T. M.; Randall, J. N.; Aggawal, R. J.; Matyi, R. J.; Moore, R. J.; Wetsel, A. E. *Phys. Rev. Lett.* **1988**, 535. Temkin, H.; Dolan, G. J.; Panish, M. S.; Chu, S. N. G. *Appl. Phys. Lett.* **1987**, *50*, 413. Schmitt-Rink, S.; Miller, D. A. B.; Chemla, D. S. *Phys. Rev. B* **1987**, *35*, 8113. Kayanuma, Y. *Phys. Rev. B* **1988**, *38*, 9797, and references therein.

(3) Ozin, G. A.; Stein, A.; Kupperman, A. *Adv. Mater.* **1989**, *101*, 374. Brus, L. E. *J. Mater. Res.* **1989**, *4*, 704, and references therein.

(4) Ozin, G. A.; Stein, A.; Stucky, G. D.; Godber, J. G. *J. Inclusion Phenom.*, in press. Ozin, G. A.; Stein, A.; Godber, J. G. U.S. Patent 4,942,119, July 1990. Wang, Y.; Herron, N. *J. Phys. Chem.* **1987**, *91*, 257. Herron, N.; Wang, Y.; Eddy, M. M.; Stucky, G. D.; Cox, D. E.; Moller, K.; Bein, T. *J. Am. Chem. Soc.* **1989**, *111*, 530. Moller, K.; Eddy, M. M.; Stucky, G. D.; Herron, N.; Bein, T. *J. Am. Chem. Soc.* **1989**, *111*, 2569. Wang, Y.; Herron, N. *J. Phys. Chem.* **1987**, *91*, 5005; *Ibid.* **1988**, *92*, 4988. Thomas, J. K.; Stramel, R. D.; Nakamura, T. *J. Chem. Soc., Faraday Trans. 1* **1988**, *84*, 1287. Parise, J. B.; MacDougall, J.; Herron, N.; Farlee, R.; Steight, A. W.; Wang, Y.; Bein, T.; Moller, K.; Moroney, L. M. *Inorg. Chem.* **1988**, *27*, 221. Terasaki, O.; Yamazaki, K.; Thomas, J. M.; Ohsuna, T.; Watanabe, D.; Sanders, J. V.; Barry, J. C. *Nature* **1987**, *330*, 58. Bogomolov, V. N.; Kholodkevich, S. V.; Romanov, S. G.; Agroskin, L. S. *Solid State Commun.* **1983**, *47*, 181. Tamura, K.; Hosokawa, S.; Endo, H.; Yamasaki, S.; Oyanagi, H. *J. Phys. Soc. Jpn.* **1986**, *55*, 528.

(5) Barrer, R. M.; Kanellopoulos, A. G. *J. Chem. Soc. A* **1970**, 766; *Ibid.* **1970**, 775.

0022-3654/90/2094-7562$02.50/0

The notation used in this equation is as follows: M, a univalent extraframework cation; OZ, the charge-balancing zeolite framework; g, the gas phase; a, the adsorbed state; i, intrazeolite confined; o, external zeolite crystal surface located MX clusters, respectively. Barrer proposed that the physical sorption of $(HX)_a$ and the chemistry of ion exchange depends on the temperature and choice of cation.[5] Depending on whether the salt created within the zeolite exists in a molecularly dispersed form as ion pairs or aggregated into intracrystalline or external surface clusters $m(MX)_{o,i}$, the sorption isotherms will be of the reversible or irreversible type.[5] For zeolites having Si/Al > 2.5, the lattice integrity was essentially maintained up to 600 °C.[5] It is surprising that no details of the reorganization process that results in the occluded salt have been reported since Barrer's pioneering work in this area. However, in an even earlier study (1965–70) Angell and co-workers noted that anhydrous HCl places a proton on the oxygen of the zeolite framework while the coexisting chloride anion is most likely associated with the extraframework cation.[6] With this as background material, it is apparent that to create monodispersed intrazeolite halide, sulfide, or phosphide quantum crystallites using HX, H_2S, and PH_3 reactions with MZ, one must define and document the parameters that influence the sorption/desorption, ionization, charge-separation, ion-exchange, and aggregation processes that occur in the zeolite. As a first step toward quantification of this kind of chemistry, we report an investigation of the reactions of anhydrous hydrogen halides HX (where X = Cl, Br, I) with a range of extraframework cation-modified versions of zeolite Y. This study leads to a class of microporous materials that can be described as "proton-loaded zeolites" or "packaged acids", which will be demonstrated to represent an archetype on the road to "packaged insulators and semiconductors".[3,4]

Experimental Section

Materials: Superior-quality sodium zeolite Y was supplied by Union Carbide, Tarrytown, NY, and was determined by powder X-ray diffraction (XRD) to be highly crystalline. Elemental analysis gives the unit cell composition $Na_{56}(AlO_2)_{56}(SiO_2)_{136}xH_2O$ for the zeolite Y. Various acid zeolites H_nNa_{56-n}–Y (where n = 0, 8, 16, and 56) and other alkali-metal zeolite Y samples were prepared from Na_{56}–Y by use of standard ion-exchange techniques of the type described by, for example, Breck[8] and Dwyer and Dyer.[20] The removal of Brønsted acid sites in as-supplied Na_{56}–Y is achieved by washing with 0.1 N NaOAc and checked in the dehydrated zeolite by the flatness of the baseline in the ν(OH) and δ(OH) regions of the mid-IR spectrum.

Anhydrous hydrogen halides and methyl halides were of research grade (Canadian Liquid Air) and were used without any further purification. Anhydrous deuterium halides were obtained from Matheson.

Spectroscopic cells and equipment: The mid-IR cell used here basically consists of a Pyrex tube with NaCl infrared windows at one end joined via a metal O-ring-sealed flange to a quartz dehydration tube at the other end.[9] The zeolite wafers are supported in a stainless steel holder that can be conveniently slid from the furnace zone to the mid-IR observation part.

The mid/far-IR cell was designed to study the wafer before and after in situ treatment with hydrogen halides by using both the mid- and far-IR probe.[7] The cell basically consists of a quartz tube with NaCl windows at one end (mid-IR part) joined to a stainless steel part with polyethylene windows at the other end (far-IR part) via a stainless steel flange. The stainless steel zeolite wafer holder can be moved easily from the dehydration zone to either the mid- or far-IR part to take the respective spectra of the same sample at each stage of the study.

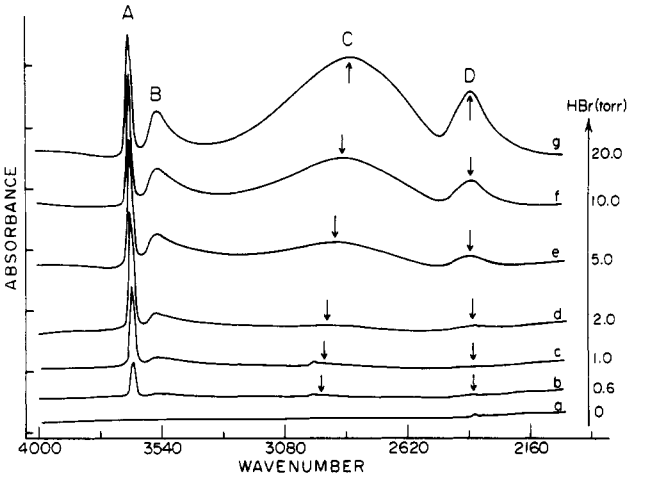

Figure 1. Sorption of anhydrous HBr into dehydrated $Na_{56}Y$: (a–g) Increasing HBr pressure.

Methods: About 20 mg of monodispersed zeolite crystals is pressed into a self-supporting wafer with a diameter of 16 mm by applying a pressure of 5 tons/in.^{2} for 10 s. The disks are secured in the stainless steel sample holder and placed in the quartz part of the cell. The thermal dehydration/deammination of the wafer under dynamic vacuum, using an Omega Series CN-2010 programmable temperature controller, follows a preset temperature schedule: 25–100 °C over 1 h, 1 h at 100 °C, 100–450 °C over 3 h, and 1 h at 450 °C. This was followed by calcination in a static atmosphere of 300 Torr of oxygen at 450 °C for 1 h and pumping hot at this temperature. The degree of dehydration was judged by the flatness of the baseline in the IR ν(OH) stretching and δ(OH) deformation regions, 3400–3700 and 1600–1650 cm^{-1}, respectively. The degree of deammination was judged by observing the sharp ν_{OH} bands at about 3640 and 3530 cm^{-1} for the α-cage and β-cage Brønsted acid sites, respectively. When a sufficiently dehydrated sample was obtained, the wafer was exposed to the anhydrous hydrogen halide under a given pressure until an equilibrium pressure had been reached. Exposure times varied from a few seconds for HCl and HBr to 2 min for HI. Further thermal treatments were carried out under dynamic vacuum using a temperature-controlled furnace. Exchange reactions were carried out with DX on the $(HX)_n/Na_{56}Y$ or $H_nNa_{56-n}Y$ systems prepared in a similar manner.

HBr loadings: Quantification of the degree of protonation of the zeolite Y was determined by neutron activation analysis at the University of Toronto Slowpoke Reactor Facility. The analysis was carried out on the protonated samples having essentially no excess hydrogen bromide (see section v). By assuming that $[Br]^- = [OH]^+$, the number of protonated oxygen sites per unit cell could be determined by counting $^{80}_{35}Br$ (617 keV, half-life 17.8 min) and $^{28}_{13}Al$ (1778.9 keV, half-life 2.24 min) in the irradiated sample.

Spectrometers: The mid- and far-IR spectra were obtained on Nicolet 20 SXB FTIR and 20F FTIR spectrometers, respectively.

The ^{27}Al and ^{29}Si MAS NMR spectra were obtained on a General Electric GN-300 (78.3 MHz for ^{27}Al and 59.7 MHz for ^{29}Si) instrument equipped with Chem Magnetic MAS probe by using KELEF rotors at speeds up to 5.0 kHz. The 90° pulse width is 3.6 μs. Chemical shifts are referred to aluminum nitrate and tetramethylsilane.

Powder XRD data were collected on a Scintag PADX X-ray diffractometer with θ–θ geometry and using Cu Kα radiation at a scan rate of 2°/min with a resolution set at 0.03° and silicon powder employed as an internal reference.

Results and Discussion

$Na_{56}Y$/HBr. The General Picture. The ν(OH) mid-IR region of a defect-removed (aqueous NaOAc washed; see Experimental

(6) Angell, C. L.; Schaffer, P. C. *J. Phys. Chem.* **1965**, *69*, 3463. Angell, C. L.; Howell, M. V. *J. Phys. Chem.* **1970**, *74*, 2737.
(7) Ozin, G. A.; Baker, M. D.; Godber, J. G. *J. Phys. Chem.* **1989**, *93*, 2899, and references therein.
(8) Breck, D. W. *Zeolite Molecular Sieves*; Wiley: New York, 1984. Barrer, R. H. *Hydrothermal Chemistry of Zeolites*; Academic Press: New York, 1982.
(9) Ozin, G. A.; Godber, J. G. *J. Phys. Chem.* **1988**, *92*, 4980; *Ibid.* **1988**, *92*, 2841.

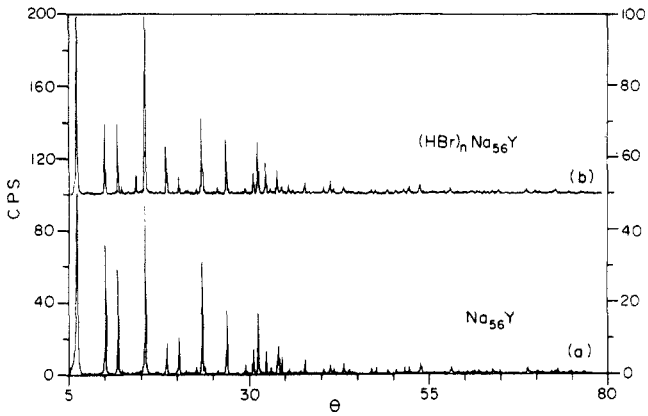

Figure 2. High-resolution powder XRD results for (a) dehydrated $Na_{56}Y$ and (b) $Na_{56}Y$ saturated with HBr at room temperature. Note that following a 300 °C vacuum thermal desorption of HBr from sample (b) the powder XRD pattern reverts exactly to that of the parent $Na_{56}Y$ sample shown in (a).

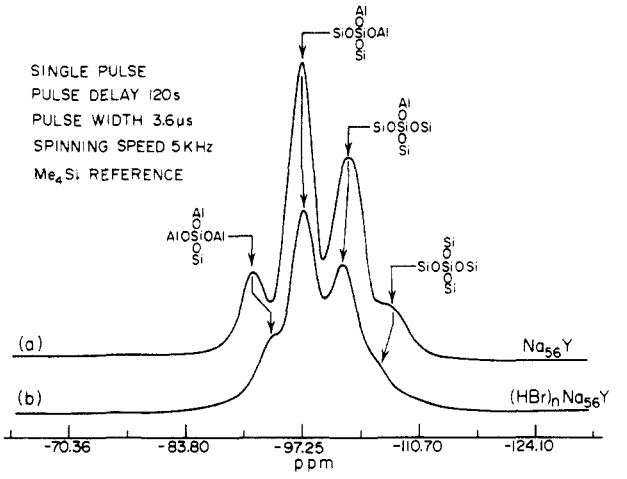

Figure 3. ^{29}Si MAS NMR spectra of (a) dehydrated $Na_{56}Y$ and (b) $Na_{56}Y$ saturated with HBr. Note that following a 300 °C vacuum thermal desorption of HBr from sample (b), the ^{29}Si MAS NMR spectrum reverts exactly to that of the parent $Na_{56}Y$ sample shown in (a).

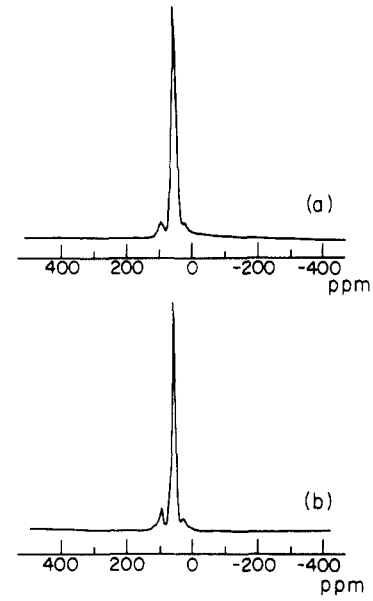

Figure 4. ^{27}Al MAS NMR spectra of (a) dehydrated $Na_{56}Y$ and (b) $Na_{56}Y$ following room-temperature sorption and 300 °C vacuum thermal desorption of HBr.

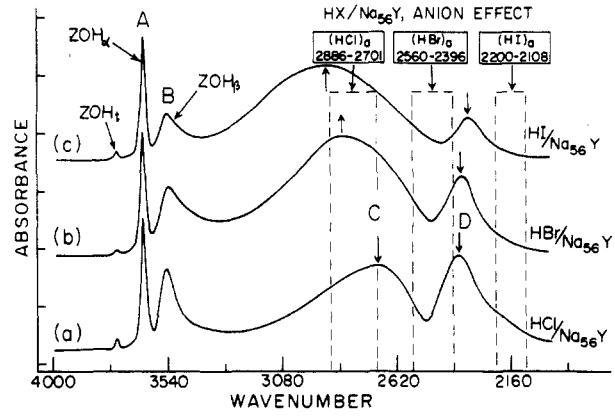

Figure 5. Sorption of high loadings of anhydrous (a) HCl, (b) HBr, and (c) HI into dehydrated $Na_{56}Y$.

Section), fully Na^+ cation exchanged, calcined and rigorously vacuum thermally dehydrated $Na_{56}Y$ self-supporting wafer is completely devoid of absorptions ascribable to Brønsted acid sites or adsorbed water (Figure 1a). On exposing the wafer to progressively increasing pressures of anhydrous HBr (Figure 1b–g), one observes the evolution of four main absorptions centered around 3647, 3544, 2804, and 2363 cm^{-1} denoted A–D, respectively. Only the C absorption appears to display small but measurable monotonically increasing red-shifts with increasing pressure of HX. The growth/decay behavior of these four absorptions clearly defines the existence of *three* distinct species, namely, those corresponding to A, B, and C/D. Thus with increasing HBr pressure, species A first grows in and then decays, while species B and C/D simply continue to grow in at distinctly different rates (see later). The effect of a vacuum thermal treatment of the sample shown in Figure 1g provides additional support for the proposal of the existence of *three* distinct species in the $Na_{56}Y$/HBr wafer. Here one observes the progressive loss of absorption C/D beginning around 100 °C, followed by B around 150 °C, with first growth of A around 150 °C and then monotonic decay around 200 °C, until the mid-IR spectrum is again completely free of absorptions (Figure 1a). The aforementioned adsorption/desorption effects are completely reversible and reproducible in the same sample (numerous times) as well as from sample to sample of $Na_{56}Y$. The XRD patterns and ^{29}Si and ^{27}Al MAS NMR spectra of the $Na_{56}Y$/HBr samples (representative examples are displayed in Figures 2–4) remain essentially unchanged throughout the entire series of operations described above (see later), establishing that the degree of crystallinity and integrity of the zeolite Y lattice is maintained with no detectable signs of dealumination throughout the adsorption and thermal desorption processes (in accordance with Barrer's and Angell's original 1965–1970 observations[5,6]). It is worth mentioning here that a unit cell analysis of high-resolution X-ray powder data for $Na_{56}Y$ and $(HBr)_nNa_{56}Y$ shows essentially no alteration in the host zeolite Y unit cell edge dimension (24.690 (2) Å) from zero to saturation loadings of HBr (see later). Entirely analogous growth and decay behavior is observed for the anhydrous $HX/K_{56}Y$ system with the exception of (a) small frequency shifts on bands A–D compared to $HX/Na_{56}Y$, (b) the requirement of a roughly 100 °C higher temperature to achieve the same thermal desorption effects as found for $HX/Na_{56}Y$, and (c) the predominance of the C/D bands over the A and B bands from early on in the HX sorption process (see part 2, Figure 12 for details).

$Na_{56}Y$/HX. The Effect of Changing the Halogen. The species formed on exposing $Na_{56}Y$ to HX (X = Cl, Br, I) display remarkably similar mid-IR spectra during both adsorption and thermal desorption (Figures 5 and 6). Species A, B, and C/D exist for all three hydrogen halides, the most noticeable spectral difference being associated with species C/D. One observes a dramatic blue-shift in absorption C on passing from HCl to HBr to HI with a concomitant small red-shift in absorption D (Figure 5a–c). Absorptions A and B for all three hydrogen halides occur at essentially identical frequencies (Figure 6) and very close to those of the characteristic ν(OH) modes of the α- and β-cage

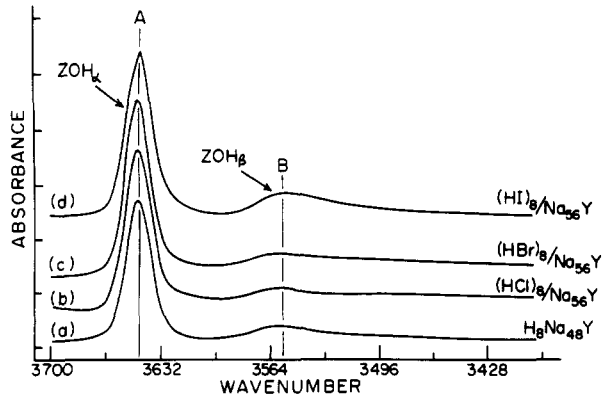

Figure 6. α- and β-cage ν(OH) IR absorptions for (a) $H_8Na_{48}Y$ and low loadings of (b) $(HCl)_8Na_{56}Y$, (c) $(HBr)_8Na_{56}Y$, and (d) $(HI)_8Na_{56}Y$.

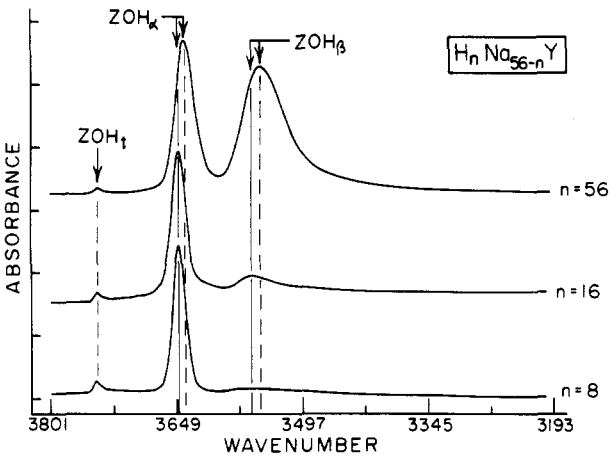

Figure 7. α- and β-cage ν(OH) IR absorptions for (a) $H_8Na_{56}Y$, (b) $H_{16}Na_{40}Y$, and (c) $H_{56}Y$.

Brønsted acid sites found in $H_{56}Y$, $H_{16}Na_{40}Y$, and $H_8Na_{48}Y$ (Figure 7; see later).

$Na_{56}Y/HX/DX$. The Effect of H/D Isotopic Substitution. When roughly 1:1 HCl/DCl and HBr/DBr mixtures are exposed to a $Na_{56}Y$ wafer under low-pressure conditions, two main mid-IR absorptions grow in, one in the ν(OH) region corresponding to species A and one in the ν(OD) region showing the characteristic $(\mu(OD)/\mu(OH))^{1/2}$ isotopic shift expected on passing from an essentially decoupled OH to an OD diatomic harmonic oscillator (Figure 8b,c). The frequencies of these ν(OH)/ν(OD) absorptions are essentially invariant to the choice of hydrogen halide and are the same as those observed for the α-cage Brønsted acid OH/OD sites in a mixed $H_4D_4Na_{48}Y$ sample (Figure 8a).

$Na_{56}Y/HBr$. Adsorption-Induced Far-IR Cation Shifts. The far-IR spectrum of the dehydrated $Na_{56}Y$ self-supporting wafer shown in Figure 9a clearly displays four resolved absorptions below 200 cm^{-1} diagnostic of translatory motions of Na^+ cations located in sites II (α-cage), I (hexagonal prism), I′ (β-cage), and III (α-cage).[7] Pore-opening framework modes occur above 200 cm^{-1} and are denoted F in Figure 9. On exposing the wafer to 5 Torr of HBr, one observes small, reproducible blue-shifts of 5–10 cm^{-1} *only* on the α-cage Na^+ cations in sites II and III (Figure 9b). The frequencies of the modes corresponding to Na^+ cation translations in inaccessible β-cage site I′ and hexagonal prism site I (see later) remain essentially invariant to the HBr adsorption process (Figure 9). Thermal desorption of HBr from the $Na_{56}Y$ wafer essentially reinstates all of the Na^+ cation modes to their original values in the virgin sample (Figure 9c–e). This process can be reproduced numerous times in the same $Na_{56}Y$ sample, as well as from $Na_{56}Y$ sample to sample without any noticeable differences. These far-IR spectral alterations on adsorption and desorption of HBr by $Na_{56}Y$ signal a scheme involving weak reversible adsorption on substantial proportions (homogeneity ideas; see later) of the accessible α-cage Na^+ cation sites, rather than a process of ion exchange and occluded salt formation, as alluded to in Barrer's work.[5]

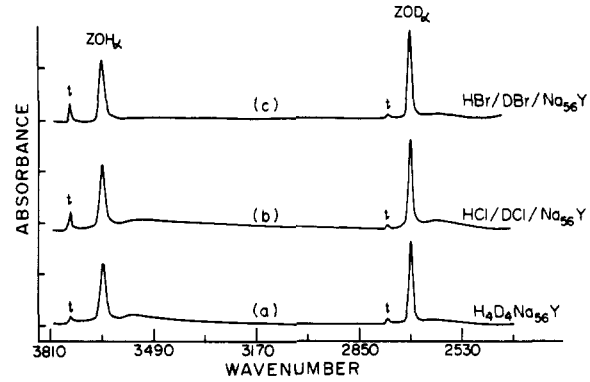

Figure 8. α- and β-cage ν(OH)/ν(OD) IR absorptions for (a) $H_4D_4Na_{48}Y$, (b) $(HCl)_4(DCl)_4Na_{56}Y$, and (c) $(HBr)_4(DBr)_4Na_{56}Y$.

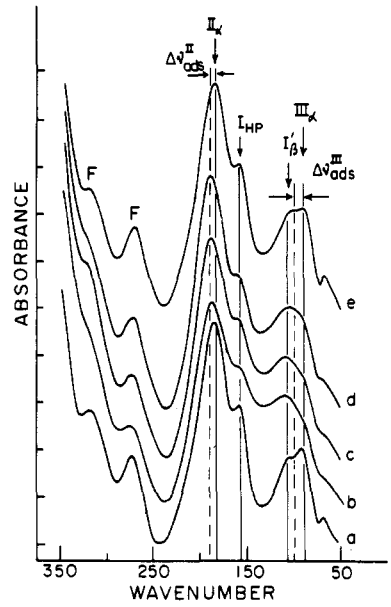

Figure 9. Far-IR spectra of (a) dehydrated $Na_{56}Y$ and (b) $(HBr)_8Na_{56}Y$ followed by thermal vacuum treatment of $(HBr)_8Na_{56}Y$ at (c) 120 °C (d) 170 °C, and (e) 450 °C each for 1 h.

$Na_{56}Y/HX$. The Proposed Model. With the experimental information described above a zeroth-order model can be proposed that fits the main observations for the reversible adsorption–desorption of anhydrous HX in $Na_{56}Y$. The model will first be presented and then followed with an extensive series of experiments designed to further test the proposed model as well as to extract more intricate details of the processes involved on adding HX to and removing HX from $Na_{56}Y$. The model to be evaluated can be described as (i) α-cage confined HX, (ii) adsorption, cation-induced ionization, and charge separation of HX, (iii) formation of α- and β-cage Brønsted acid sites, (iv) formation of α-cage $Na^+\cdots X^-$ contact ion-pairs, and (v) solvation of Brønsted acid sites by HX.

(i) α-Cage Confined HX in $Na_{56}Y$. The kinetic diameters of HX (3.2–3.8 Å) imply that room-temperature entry through a 2.3-Å diameter six-ring window to the β-cage and through a 1.6-Å diameter four-ring window to the hexagonal prism are most unlikely events.[8] Strong support for this argument is found in the far-IR observation of exclusively α-cage Na^+ cation adsorption-induced frequency shifts (Figure 9). Another approach to this question involves experiments involving the reaction of HX with dehydrated sodium hydroxosodalite, a felspathoid built "entirely" of close-packed β-cages. The contents of each β-cage can be described as a centrally located hydroxide anion, surrounded tetrahedrally by four Na^+ cations, each in close association with three oxygens of a six-ring charge-balancing site (Figure 10).[8]

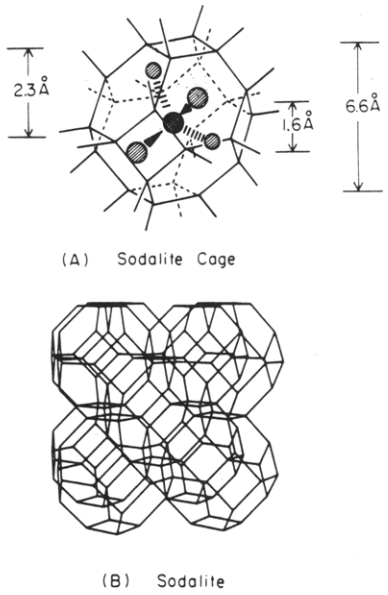

Figure 10. (A) Sodalite cage of SiO_4^{4-} and AlO_4^{5-} tetrahedra with a M_4X tetrahedron at the center. (B) Stereoplot of the unit cell of sodalite showing the close packing of β-cages (cubooctahedra) in the sodalite structure.

The basic principle behind this experiment can be described in the equation

$$\text{Na,OH–SOD} + \text{HX} \rightarrow \text{Na,X–SOD} + \text{H}_2\text{O}$$

If for example, HBr can gain access to the sodalite cages at room temperature, then sodium hydroxosodalite will transform to sodium bromosodalite (distinct far-IR phonon spectra and unit cell dimensions) with the concomitant formation of H_2O (mid-IR detectable) confined to the external surface of the crystals. In practice one finds that no reaction occurs at room temperature. At 150 °C, one observes the formation of H_2O (mid-IR) and NaBr crystals (XRD) without any sign of Na,Br–SOD (far-XRD[9]). The lattice integrity of the Na,OH–SOD is maintained throughout all of these operations (IR, XRD).[9] Clearly these observations reveal the existence of only an external surface reaction of crystalline Na,OH–SOD with HBr to produce surface-adsorbed H_2O and externally confined bulk NaBr with no evidence for penetration of HBr into the internal regions of the sodalite lattice. Taken together, the above information provides a fairly convincing case for the containment of HX in the α-cage of $Na_{56}Y$ at room temperature.

(ii) Adsorption, Cation-Induced Ionization, and Charge Separation of HX in $Na_{56}Y$. The comprehensive studies of the isotherms of anhydrous HCl in dehydrated $Na_{56}Y$ at 190–320 °C clearly depict a process involving reversible physical sorption and irreversible ion exchange as mentioned in the Introduction.[5] The dramatic creation of characteristic ν(OH) mid-IR absorptions displaying diagnostic ν(OH)/ν(OD) isotopic frequency shifts (and isotope-exchange behavior; see later) and bearing a striking resemblance to α- and β-cage Brønsted acid sites in $H_nNa_{56-n}Y$ (Figures 5–7) provides unequivocal evidence for ionization of HX in $Na_{56}Y$ followed by protonation of lattice oxygen sites. That the ionization/protonation step is induced by the polarization of the HX molecule via the high electrostatic field associated with the exposed α-cage Na^+ cations[10] receives considerable support from the absence of this process in $H_{56}Y$, ALPO-5, and SiO_2-Y described later. The proposal of charge and spacial separation of protonated oxygen lattice sites from the associated halide anion stems from two key experimental findings. First, the invariance of ν(OH) to changes in the halide from Cl to Br to I strongly suggests that proton–halide charge separation has ensued following cation-induced ionization of HX in $Na_{56}Y$. Second, the observation of small and reproducible perturbations on the far-IR Na^+ cation translatory modes associated with α-cage site II and III cations (Figure 9) provides direct evidence that the halide anion is almost certainly associated with the Na^+ cations, most likely as a contact ion pair. Taken together, the above information provides a consistent picture for adsorption, cation-induced ionization, and charge separation of HX in $Na_{56}Y$.

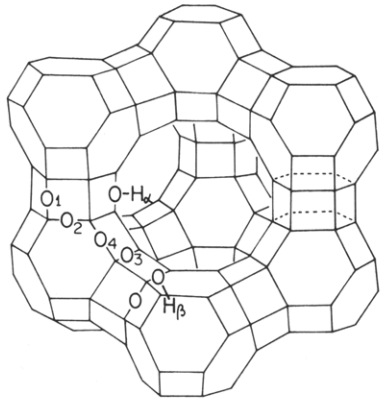

Figure 11. Portion of the faujasite unit cell, showing framework oxygen numbering and α- and β-cage Brønsted acid site locations and designations.

(iii) Formation of α and β-Cage Brønsted Acid Sites from HX in $Na_{56}Y$. (a) Preamble: Brønsted Acid Zeolites. Before embarking on this discussion, let us briefly review the features of Brønsted acid zeolites that are most pertinent to the present study. To begin, Brønsted acid sites in zeolites are normally produced by dilute aqueous acid exchange of alkali-metal zeolites, deamination of ammonium zeolites, hydrolysis of zeolitic water by multivalent cations, and redox reactions of adsorbed molecules.[8,10]

In the specific case of $H_nNa_{56-n}Y$ a combination of neutron diffraction, ^{1}H NMR, and mid-IR spectroscopy have established the locations and populations of the protons over the full range of substitution of Na^+ cations by protons.[11] The protons of the structural OH groups are attached to the Al–O–Si bridging oxygens, lying in the Al–O–Si plane on an axis bisecting the Al–O–Si angle at about 1 Å from the oxygen. Direct evidence of this picture stems from neutron diffraction from which the number and type of OH group per unit cell of Y type zeolites have been established. The protons are located on O(4), O(3), O(2), and O(1) in the faujasite type structure (Figure 11). The maximum number of each of these oxygen sites in the unit cell is 96; however, charge-balance and proton–proton repulsions greatly limit the maximum number of protons found at each oxygen lattice site. At small proton contents ($n < 8$) Na^+ on sites I and I′ prevent the formation of O(3)–H (lying in the β-cage, directed toward site I′) and O(1)–H is the preferred OH group (lying in the α-cage, directed toward the cage center). As the Na^+ content is decreased ($n > 8$) the β-cage proton population begins to grow, together with that of the α-cage protons; eventually at close to full Na^+ exchange the majority of protons are located in the β-cage. The classic neutron diffraction papers of Olsen et al. and Smith et al.[12] established the number and type of OH groups per unit cell in $H_{58}Y$ to be

$$\text{O(1)–H} = 17;\ \text{O(2)–H} = 10;\ \text{O(3)–H} = 28;\ \text{O(4)–H} = 3$$

giving an α:β cage content of 27:31.

The pioneering mid-IR studies of Ward and others[10] have established in detail the vibrational characteristics of α- and β-cage Brønsted acid sites in faujasites. The fundamental stretching vibration of the α- and β-cage OH groups in faujasites always fall in a narrow range close to 3650 and 3550 cm^{-1}, respectively. The small variations in these diagnostic ν(OH) frequencies that

(10) *Zeolite Chemistry and Catalysis*; Rabo, J., Ed. ACS Symp. Ser. **1976**, *171*, 118.

(11) Mortier, W. J.; Schoonheydt, R. A. *Prog. Solid State Chem.* **1985**, *16*, 1, and references therein.

(12) Olsen, D. H.; Dempsey, E. *J. Catal.* **1969**, *13*, 221. Mortier, W. J.; Pluth, J. J.; Smith, J. V. *J. Catal.* **1976**, *45*, 367.

do accompany changes in, for example, cation type, cation number, and the aluminum content of the zeolite, can usually be traced to accompanying alterations in the electron density on the framework oxygen sites to which the proton is attached.[11]

Quantification of this idea derives from semiempirical and ab initio quantum mechanical calculations of atomic charges and overlap populations for the atomic components of representative model systems (fragments, building units) of the zeolite unit cell.[11] Another useful approach for gauging alterations in oxygen framework electron density makes use of the empirical electronegativity scale of Sanderson.[11] For a compound $P_pQ_qR_r$, the intermediate electronegativity, S_{int}, is postulated to be the geometric mean of the atomic electronegativity:

$$S_{int} = (S_P{}^p S_Q{}^q S_R{}^r)^{1/p+q+r}$$

where S_P, S_Q, and S_R are the electronegativities of the atoms P, Q, and R, respectively. This average electronegativity has been successfully applied to zeolites and appears to adequately express the influence of several important parameters in a single number.[11] The electronegativity scales tabulated in ref 11 prove to be invaluable for estimating the relative binding strengths of protons to the oxygens of the framework in variously substituted faujasites (see later).

The outstanding acidic and carboniogenic properties of zeolites makes them excellent catalysts for a wide range of size- and shape-selective hydrocarbon transformations.[8,10,11] When considering the acidity of the Brønsted acid sites in zeolites, one must remember that one is dealing with a dynamic phenomenon that in the absence of an interacting molecule (base) does not have any physical meaning. Thus acidity is normally probed by *n*-butane cracking activity, acid–base indicators, calorimetry of acid–base reactions, TPD-MS involving desorption of bases, ^1H, ^{15}N, and ^{31}P NMR of protonated amines and phosphines, and $\Delta\nu_{OH}$ bathochromic IR vibrational shifts induced by interaction with weak bases.[8,10,11] Thus it is clear that acidity cannot be separated from the interaction with molecules (we will exploit this concept for probing the acidity of proton-loaded zeolites compared to traditional Brønsted acid zeolites; see later). One cannot expect to describe the acidic properties of the zeolite OH groups using OH vibrational frequencies, force constants, and bond strength considerations. This is vividly illustrated by the higher α-cage ν(OH) compared to the β-cage ν(OH), but with the acid strengths following the *same order*! As expected however, within a particular zeolite structure type such as, faujasite, the ν(OH) stretching frequency varies linearly with the S_{int} for both the α- and β-cage protons.[11] The weakening (but not breaking) of the OH bond upon interaction with weak bases as seen in the $\Delta\nu_{OH}$ IR bathochromic shift provides a measure of acidity of the proton or proton acceptor ability of the base.[11] There exist rather good relationships between measured IR $\Delta\nu_{OH}$ shifts and proton affinities for a wide range of bases, as well as $\Delta\nu_{OH}$ and S_{int} for a range of zeolites with respect to a particular base.[11]

The dynamic aspect of acidity considers the probability of the proton jumping to the interacting molecule. This process requires proton mobility and is a property that has been investigated by NMR and electrical conductivity techniques.[11] One usually thinks in terms of a proton mean jump frequency or residence time of a proton on its oxygen. In the context of discussions of acidity, interacting molecules can be considered as vehicles, conveying the protons between oxygen framework sites. The mobility of the β-cage protons can be appreciated from its reaction with bases that are spacially too bulky to pass through the 2.3-Å diameter six-ring entrance windows to the β-cage. Measurements of the proton relaxation times directly leads to quantification of proton diffusion coefficients.[13]

(*b*) *Proton-Loaded Zeolites.* With the above synopsis as background for appreciating the properties of Brønsted acid sites in zeolites, particularly faujasites, let us now turn our attention to our proposed protonation model of $Na_{56}Y$ by HX. From inspection of Figures 1–9 there can be no doubt that the sorption

SCHEME I

SORPTION, IONIZATION CHARGE-SEPARATION MODEL

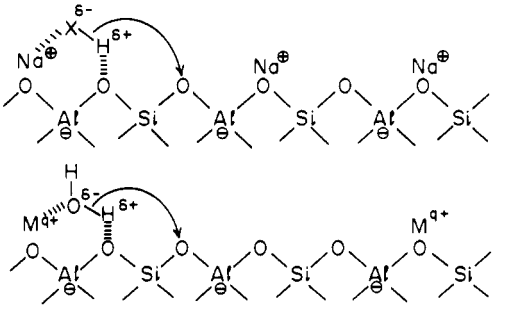

THE PARALLEL BETWEEN HX AND H_2O

of anhydrous gaseous HX into dehydrated $Na_{56}Y$ protonates oxygen sites in the zeolite framework, leaving the extraframework Na^+ cations essentially in their original lattice sites of the virgin $Na_{56}Y$. Especially noteworthy are the essentially identical frequencies and line shapes of species A and B to those of α- and β-cage Brønsted acid sites in $H_nNa_{56-n}Y$ (where n = 8, 16; see later and Figures 5 and 6). Significant also are the absence of a measureable halide effect on species A and B (Figure 5) and the exclusive perturbation of α-cage Na^+ cation far-IR translatory modes (Figure 9).

It would appear therefore that species A and B are best described as protonated oxygen framework sites, bearing a "striking resemblance" to normal α- and β-cage Brønsted acid sites. However, whether or not protonated oxygen framework sites are actually identical with Brønsted acid sites has yet to be substantiated. This question will be addressed in detail by using solvation, acidity, mobility, H/D exchange, S_{int} and desorption kinetic probes; see later.

(*iv*) *Formation of α-Cage $Na^+\cdots X^-$ Contact Ion Pairs.* The polarization, ionization and charge-separation process for HX in $Na_{56}Y$ is envisaged to be induced by the huge electric fields associated with the Na^+ cations (Rabo's expanded ionic lattice ideas[10]). This process clearly bears some considerable similarity to the ionization of a zeolitic water molecule coordinated to an extraframework multivalent cation.[8] A likely model for the adsorption, polarization, ionization, and charge separation for both HX and H_2O is illustrated in Scheme I. The dipolar nature of HX demands that the halide end of the molecule will preferentially interact with the Na^+ cation, with the proton end interacting with the framework oxygen. A similar scheme also applies to H_2O; however, the lower polarity and acidity of H_2O relative to HX necessitates that only the higher electrostatic field of a multivalent cation will be sufficient to induce ionization of H_2O and charge separation of the hydroxide from the proton. Neutron diffraction data provide definitive support for this model in the case of M^{2+} and M^{3+} cation induced hydrolysis of zeolitic water.[8,14] Here the hydroxide anion is found to be associated with the cation as a contact ion pair while the released proton resides on a framework oxygen. Reaction with bases demonstrate the Brønsted basic nature of the $M^{q+}OH$ hydroxide and the Brønsted acidic nature of the ZOH proton. Clearly the cation-induced hydrolysis of intrazeolite water sets a precedent for the type of polarization, ionization, and charge separation events that are envisaged for anhydrous hydrogen halides in $Na_{56}Y$. In particular it suggests that the halide anion is most likely associated with the polarizing cation that caused the actual ionization process to occur in the first place. Two pieces of experimental evidence support the proposal of a contact $ZONa^+\cdots X^-$ ion pair for the $HX/Na_{56}Y$

(13) Pfeifer, H.; Freude, D.; Hunger, M. *Zeolites* **1985**, *5*, 274.

(14) Cheetham, A. K.; Eddy, M. M.; Thomas, J. M. *J. Chem. Soc., Chem. Commun.* **1984**, 1337, and references therein.

system. First, only the α-cage Na^+ site II and III cations are weakly perturbed as seen from their far-IR translatory mode frequency shifts, following HX ionization and charge separation, indicating the presence of a weakly interacting halide anion alongside the cation (Figure 9 and see earlier discussion). Second, the exclusive solvation of the α-cage proton by HX rather than the α-cage Na^+ cations (see the following section) implies that the cation sites are blocked by the neighboring anion. Taken together, the above considerations provide a fairly convincing case for the formation of α-cage $ZONa^+\cdots X^-$ contact ion pairs.

(v) *Solvation of Brønsted Acid Sites by HX.* Having pinpointed species A and B as protonated α- and β-cage oxygen framework sites with the accompanying anion most probably existing as contact ion pairs with α-cage Na^+ cation partners, we now direct our attention to the nature of the remaining species of interest, denoted as C/D. As delineated earlier, this species displays monotonic growth behavior with increasing loading of HX into $Na_{56}Y$, in unison with the concomitant growth of species A and B, the α- and β-cage protonated oxygen sites followed by the decay of species A. As described earlier, thermal desorption of HX cleanly reverses this process (see later).

Points of special interest concerning species C/D are as follows (Figures 1 and 5): (a) large bathochromic shifts $\Delta\nu_{OH}$ with respect to the unperturbed $\nu(OH_\alpha)$; (b) a broad, structured C band; (c) large halide-dependent shifts for the C band, $\Delta\nu(HCl) > \Delta\nu(HBr) > \Delta\nu(HI)$; (d) small halide-dependent shifts for the D band, $\Delta\nu(HCl) < \Delta\nu(HBr) < \Delta\nu(HI)$; (e) small HX loading-dependent red-shifts for the C band; (f) characteristic H/D vibrational isotope shifts for both the C and D band.

With this information, possible candidates for species C/D include (i) hydrogen-bonded $(HX)_n$ clusters, (ii) solvated protons attached $ZOH\cdots(X-H)_n$ or detached $H^+(X-H)_n$, (iii) solvated cations attached $ZONa^+\cdots(X-H)_n$ or detached $Na^+(X-H)_n$, and (iv) solvated anions attached $ZONa^+X^-\cdots(X-H)_n$ or detached $X^-(H-X)_n$.

On the basis of the following arguments, we will present a case that strongly favors the attached solvated proton description $ZOH\cdots(X-H)_n$ for species C/D.

To begin, the association characteristics of the hydrogen halides have been extensively examined in rare-gas matrices by vibrational spectroscopy.[15] Diagnostic frequency ranges for HX on passing from monomer to multimer are given here and indicated in Figure 5: $(HCl)_n$, 2886–2701 cm^{-1}; $(HBr)_n$, 2560–2396 cm^{-1}; $(HI)_n$, 2220–2108 cm^{-1}. Clearly the frequencies and halide dependence of the C band cannot be reconciled in terms of hydrogen-bonded $(HX)_n$ clusters. They are outside of the acceptable range and show the wrong dependence on halide mass. The solvation of cations in zeolite Y by water has been investigated by far-IR spectroscopy.[7,16] With increasing loading of H_2O, the usually well-resolved far-IR cation translational modes typically display large alterations in frequency, intensity, and line width. Full cation solvation is recognized by a very broad, structured far-IR feature centered in the range 100–200 cm^{-1} for most cations studied[7,16] and is ascribed to intrasupercage translational/vibrational motions of the aquated $M(H_2O)_n^+$ cation. This is in striking contrast to the behavior observed in the far-IR spectra of $HX/Na_{56}Y$ with increasing loading of HX. Instead one notices only small, α-cage Na^+ site-specific adsorption shifts rather than the much more dramatic effects expected for supercage modes of solvated $M(HX)_m^+$ species, by comparison with $M(H_2O)_n^+$ above. These minor adsorption-induced shifts are believed to arise from the proposed weakly interacting cation–anion pair rather than solvation of the cation by HX (in other words the anion blocks the cation from solvation by HX).

The argument against a solvated anion involves a comparison of the data for $HX/Na_{56}Y$ with those of $HX/H_{56}Y$. The reaction of anhydrous HX with a fully exchanged Brønsted acid zeolite

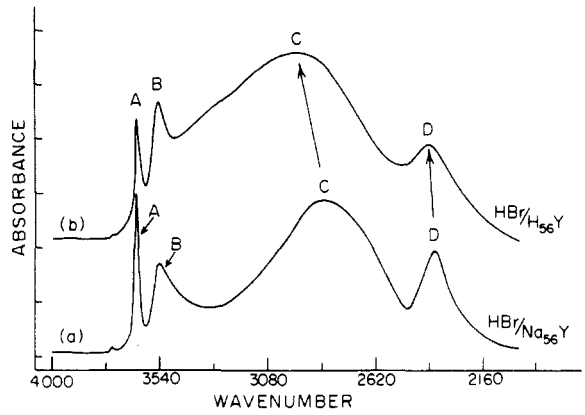

Figure 12. Mid-IR spectra of (a) $HBr/Na_{56}Y$ and (b) $HBr/H_{56}Y$.

Y as a function of HX loading is shown in Figures 1–3 in part 3 of this study. Here one does *not* observe protonation of oxygen framework sites. Instead one notes just the monotonic depletion of *both* α- and β-cage Brønsted acid sites with the concomitant smooth growth of a new species with mid-IR spectral characteristics that bear a striking resemblance to those of species C/D formed in $HX/Na_{56}Y$ (Figure 12). Details of the $HX/H_{56}Y$ system will be presented later. For the purpose of the present discussion, suffice to say that the $HX/H_{56}Y$ result reasonably eliminates the solvated anion model. Clearly protons alone can lead only to "nonproductive" HX ionization (see later). Therefore charge separation and oxygen lattice protonation cannot occur in the $HX/H_{56}Y$ system, and contact ion pairs do not exist. Hence anion solvation is not even a possibility in the $H_{56}Y$ system. Thus by a process of elimination it appears that the solvated proton model alone is the most likely contender for the assignment to species C/D. So what is the experimental evidence that specifically supports the solvated proton model?

Let us consider the vibrational properties of the system in terms of an OH oscillator (protonated oxygen lattice site, internal coordinate ΔR) hydrogen bonded to the negative end of n-solvating HX dipoles (internal coordinates Δr_n) as illustrated by

$$\begin{matrix} \Delta R & \Delta r_n \\ Z\text{-}O\text{-}H\cdots(X\text{-}H)_n \end{matrix}$$

The halide-dependent shifts described earlier for bands C and D in $HX/Na_{56}Y$ (Figure 5) are certainly those expected for this kind of hydrogen-bonding model. Here the electronegativity of the halide controls the magnitude of the $\Delta\nu_{OH}$ shift (ΔR) on band C while it is the force constant of the HX bond as well as the strength of the H bond that controls $\Delta\nu_{HX}$ of band D with respect to $\nu(HX)$ of the monomer. Thus it is well documented in the hydrogen-bonding literature that $\Delta\nu_{OH}$ is an approximate measure of the strength of the H bond.[17] Thus for the solvated proton model, one expects a monotonic red-shift of $\nu(OH)$ (band C) with increasing strength of hydrogen bonding, namely $\Delta\nu_{OH}(HCl) > \Delta\nu_{OH}(HBr) > \Delta\nu_{OH}(HI)$, as observed experimentally (Figure 5). The H-bonded $\nu(OH)$ fundamental stretching mode is distinguished by its high intensity and great breadth compared to that of the free OH oscillator.[17] Large mechanical and electrical anharmonicities associated with the H bond have been shown to be responsible for these large increases in breadth and intensity of the OH fundamental.[17] It is generally accepted that the great breadth of this band is due to combination bands of the fundamental stretching mode with low-frequency stretching and/or deformational modes of the H bond, where anharmonic coupling plays an essential role in making it possible for these combination bands to appear. (Note that for solvated protons in zeolites

(15) Hallam, H. In *The Hydrogen Bond*; Schuster, P., Zundel, G., Sandorfy, C., Eds.; North Holland: Amsterdam, 1976; Vol. I–III.

(16) Ozin, G. A.; Godber, J. G.; Baker, M. D. *Catal. Rev. Sci. Eng.* **1985**, *27*, 591, and references therein.

(17) Sandorfy, C. *The Hydrogen Bond*; Schuster, P., Zundel, G., Sandorfy, C., Eds.; North Holland: Amsterdam, 1976; Vol. I–III.

(18) Couzi, M.; Cornut, J. C.; Huong, P. V. *J. Chem. Phys.* **1972**, *56*, 426. Rush, J. J.; Schroeder, L. W.; Melveger, A. J. *J. Chem. Phys.* **1972**, *56*, 2793. Nakamoto, K. *Infrared Spectra of Inorganic and Coordination Compounds*, 4th ed.; Wiley: New York, 1988.

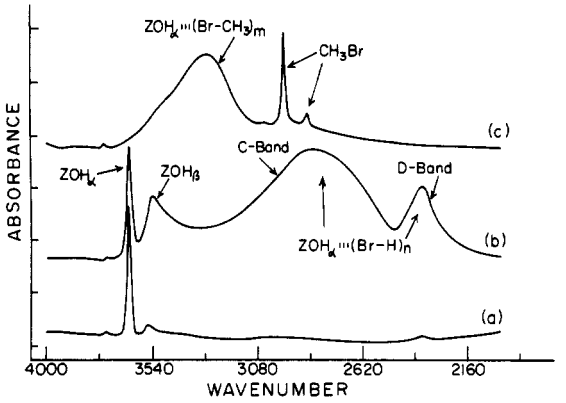

Figure 13. Mid-IR spectra of (a) low-loading $HBr/Na_{56}Y$, (b) high-loading $HBr/Na_{56}Y$, and (c) low-loading $HBr/Na_{56}Y$ in the presence of CH_3Br.

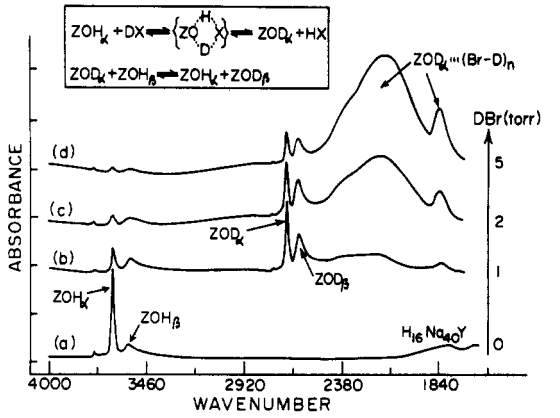

Figure 14. Mid-IR spectra of (a) $H_{16}Na_{40}Y$ and (b–d) $H_{16}Na_{40}Y/DBr$ with increasing loading of DBr.

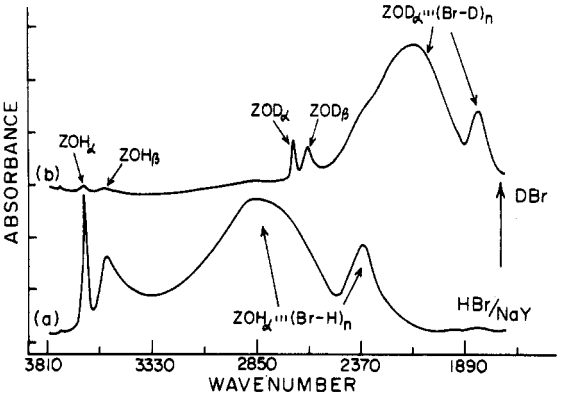

Figure 15. Mid-IR spectra of (a) $(HBr)_nNa_{56}Y$ and (b) $(HBr)_nNa_{56}Y/DBR$.

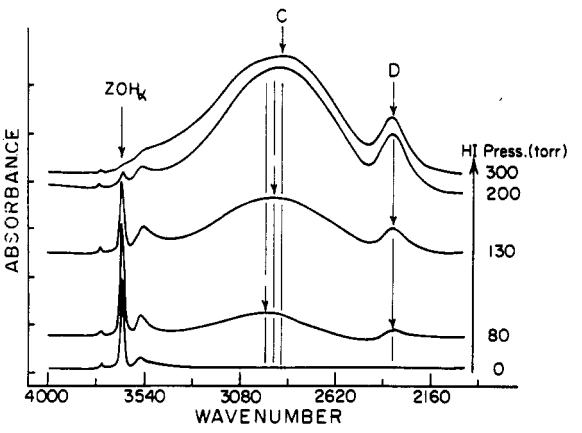

Figure 16. Mid-IR spectra of $HI/H_{16}Na_{40}Y$ at increasing pressures of HI.

inhomogeneous broadening effects probably also contribute to these great line widths, possibly having their origin in a distribution of HX solvation numbers (n) as well as slightly different microenvironments for embibed HX.)

The solvated proton model also nicely accounts for the observed small monotonic blue-shift of the proposed Δr_n mode (band D) with increasing strength of hydrogen bonding (Figure 5). On the basis of the known fundamental vibrational frequency of the HX monomer

$$HCl = 2886\ cm^{-1};\quad HBr = 2560\ cm^{-1};\quad HI = 2220\ cm^{-1}$$

one would expect the Δr_n mode to be highest for the chloride and well spaced from that of the bromide and iodide. However, because hydrogen bonding is expected to be most pronounced for the chloride, then the frequency differences between the chloride, bromide, and iodide will be reduced compared to that of the free HX molecule. It is noteworthy that compelling support for our proposed assignment of the Δr_n vibrational mode of the solvated HX moiety to band D derives from an experiment in which ZOH···$(X-H)_n$ is replaced by ZOH···$(X-CH_3)_m$ (Figure 13). Consistent with our proposed assignments for bands C and D to ΔR and Δr_n modes, one observes that band C undergoes a significant blue shift and band D disappears when HX is replaced by CH_3X as the solvating molecule. Clearly H-bonding of ZOH to HX is much stronger than to CH_3X for the series X = Cl, Br, I. Incidently, the observed bathochromic shifts $\Delta\nu_{OH}$ and band width at half-height $\Delta\nu_{1/2}$ for band C of the solvation (hydrogen bonded) series ZOH···$(X-CH_3)_m$ follow the order I > Br > Cl, which appears to track halogen nucleophilicity (polarizability) control of the H-bond strength rather than electronegativity control (see part 2 of this study, Figures 7–8). The implication is that solvation proceeds through X (see later). Note that in the H-bonding description ZOH···$(X-H)_n$ an "attached" proton model is favored from (a) the observation of a higher frequency C band than HX > H_2X^+ > HX_2^- (ref 24) and (b) the observed frequency order of the C band in the series X = Cl, Br, I (Figure 5) where the opposite order would be expected for the "detached" proton model $H^+(X-H)_n$.

Finally, the small HX loading-dependent red-shifts observed for the C band can also nicely be understood in terms of the solvated proton model. In this situation, increasing the HX solvation number n results in decreasing strength of H bonding per HX solvate, but with an overall increase in the strength of hydrogen-bond weakening of the OH bond. Therefore it is seen that the attached solvated proton model adequately accounts for all of the vibrational characteristics of species C/D.

Homogeneity of the Penetration of HX into the Zeolite Crystals. In all of our deliberations so far, it has been presupposed without experimental justification that an HX impregnation of zeolite Y involves a process in which every α-cage of the crystal is equally well accessed by the HX molecule. Because of the mobility of protons expected in these systems, the simple observation of complete H/D exchange in, for example, $H_{16}Na_{40}Y/DBr$ (Figure 14) or $(HBr)_nNa_{56}Y/DBr$ (Figure 15) does not necessarily imply that every α-cage of the crystal has been entered by DX. In fact one can readily envisage a process whereby highly active HX is strongly sorbed exclusively on the external surface layers of the zeolite crystal, never actually gaining physical entry into the bulk internal confines of the zeolite crystal. Nevertheless, one can easily imagine how protons and deuterons involved in rapid H/D hopping exchanges between oxygen framework sites could readily make their way from the outside to the inside of the crystal with the hydrogen halide remaining anchored to the external surface of the zeolite.

The definitive experiment to clarify this question involves an α-cage-selective chemical reaction that absolutely demands charge and spatial homogeneity of HX throughout the entire zeolite crystal.[19] In this context, two experiments prove to be especially

(19) Ozin, G. A.; Godber, J. G. *J. Phys. Chem.* **1989**, *93*, 878.

informative. The first involves complete solvation of α-cage Brønsted acid sites in $H_{16}Na_{40}Y$ (two protons on average per α-cage) by HX (Figure 16), and the other involves complete solvation of α- and β-cage Brønsted acid sites in $H_{56}Y$ (roughly three to four protons on average per α- and β-cage) by HX (see part 3 of this study, Figure 5). As the Brønsted acid sites in both of these systems are obliged by the strict requirement of charge balance to remain at all times, homogeneously distributed throughout the entire zeolite crystal, one is forced to the inescapable conclusion that the observation of essentially complete solvation of Brønsted acid sites by HX proves that every α-cage of the zeolite crystal is intruded by HX. This experimental realization for both $H_{16}Na_{48}Y$ and $H_{56}Y$ vindicates that indeed the penetration of HX into zeolite Y can be considered for most purposes to be homogeneous and not restricted to the external surface regions of the crystals. Throughout all of these operations, the XRD powder patterns of the samples demonstrate that the original X-ray crystallinity is maintained. That is, HX does not perturb the integrity of the zeolite lattice. In addition, the ^{29}Si and ^{27}Al MAS-NMR spectra of these same samples show no alterations diagnostic of dealumination processes with the formation of extraframework Al^{III} species.

Conclusion

In brief, the key discoveries to emerge from the study of anhydrous HX sorption by dehydrated $Na_{56}Y$ are listed here in point form: (i) α-cage confined HX; (ii) every α-cage is homogeneously accessed by HX; (iii) zeolite crystallinity and lattice integrity is maintained during the HX sorption/desorption;(iv) HX sorption, ionization, and charge-separation processes; (v) α-cage located $ZONa^+X^-$ contact ion pairs; (vi) ZOH framework protonation; (vii) α and β-cage protonation sites; (viii) rapid α- and β-cage room-temperature H/D exchange processes with DX; (ix) $ZOH_\alpha\cdots(X-H)_n$ selective α-cage proton solvation by HX; (x) H-bonding $ZOH\cdots(X-H)_n$ attached proton model with characteristic mechanical anharmonicity, electronegativity, and loading effects.

Concluding Remarks

After having read the Introduction to this paper, one might justifiably wonder what the proton-loaded zeolites of the present study have in common with the concept of creating intrazeolite semiconductor clusters by design.

Clearly the reaction of, for example, anhydrous HX, H_2S, and PH_3 with extraframework zeolite cations of various types is an important synthetic method for potentially realizing monodispersed halide, sulfide, and phosphide intrazeolite semiconductor quantum crystallites. Their relevance to quantum dot, wire, and supralattice devices has been well documented.[1-4] Important here is the realization that these "packaged or occluded semiconductors" (Barrer's terminology[8]) are being created by intrazeolite acid–base reactions (not unlike those discovered in the proton-loaded zeolites of the present study) and encapsulated/immobilized in an acidic/protonic environment. Thus in the "packaged salt" terminology, proton-loaded zeolites can be described as "packaged acids", and the results of the present study can be considered to provide many valuable clues for the design of synthetic strategies to achieve the creation and self-organization of monodisperse intrazeolite quantum crystallites.

One might also ask where all of these ideas really began? The pioneering work of Barrer and co-workers can probably be considered to represent the beginning.[8] They considered packaged salts and salt-occlusion phenomena to be akin to the "filling-up of an expanded ionic lattice", where the Madelung lattice energy term provides the stabilization driving force for the salt imbibing process. These "curious materials" found numerous interesting applications, for example, in catalysis (lattice fillers, stabilizers, enhancement of framework stability, e.g., $NaZ\{NaCl\}_n^\beta$), controlled chemical release ($NaZ\{NaClO_3\}_n$ weed killers), controlled release of gas ($NaZ\{NaClO_4\}_n/O_2$, $NaZ\{NaN_3\}_n/N_2$, $NaZ\{Al(BH_4)_3\}_n/H_2$, $NaZ\{AlCl_3\}_n/HCl$, $NaZ\{Na_2C_2O_4\}_n/CO_2$); colour centers ($NaZ\{Na_4^{3+}\}$, photochromics, cathodochromics, memory devices), and solid-state electrolytes (zeolite batteries).[8] The foresight of Barrer in envisaging something like intrazeolite semiconductors was amazing.[3] The following quotation of Barrer[8] illustrates the point well: "when the zeolite is loaded with the halide it should be possible in many instances to hydrolyse the guest species to give oxide or hydroxide and to form structures, heterogeneous on the molecular scale with oxide threads and clusters having the pattern of the channel and cavity systems and supported by the aluminosilicate framework of the zeolite. At the moment such structures remain only as chemical novelties".

In considering a synthetic strategy to intrazeolite semiconductor quantum crystallites by design, the proton-loaded zeolites of the present study can be considered to be an archetypal system:

$$\underset{(I)}{nM^+OZ + mHX(g)} \rightleftarrows m\{X^-M^+\}^\alpha m\{HOZ\}^{\alpha,\beta}(n-m)\underset{(II)}{M^+OZ} \rightleftarrows m(MX)_{o,i}m(HOZ)^{\alpha,\beta}(n-m)\underset{(III)}{M^+OZ}$$

The act of ionization and charge-separation for the proton-loaded zeolites is expressed in (II) above. Here one can see that Barrer's[5] original proposal of the nature of adsorbed $(HX)_n$ described in the Introduction to this paper must in light of the results of the present study be visualized instead as a protonated framework oxygen with a coexisting cation–anion contact ion pair, in equilibrium with HX solvated protons attached to the framework oxygen sites. The creation of occluded salt $(MX)_{o,i}$ (outside or inside surface) is couched in the transformation of (II) → (III).

Therefore it can be seen that the lesson of the $HX/Na_{56}Y$ experience is the perceived necessity to develop a deep appreciation of the factors that control sorption, desorption, ionization, charge separation, ion exchange, salt aggregation, and acid/base reactions involving HX, H_2S, and PH_3 and extraframework zeolite cations. Urgent questions that need to be addressed involve (i) the energetics and dynamics of the conversion of cation–anion contact ion pairs $m\{X^-M^+OZ\}$ to occluded salts $\{(MX)_mOZ\}$, (ii) the preferred α- or β-cage location of $(MX)_m$, and (iii) the stability of $(MX)_m$ in a protonic environment.

When extrapolating from the aforementioned ideas concerning halides to the fabrication of intrazeolite semiconductor sulfide and phosphide quantum crystallites, some intriguing additional factors must be carefully contemplated. Take, for example, the likely pathway to an embibed metal sulfide accessed through the intrazeolite reaction of H_2S with extraframework divalent cations:

$$nM^{2+}OZ + mH_2S(g) \rightleftarrows m\{H_2S\}_a nM^{2+}OZ \rightleftarrows m\{HS^-M^{2+}\}m\{HOZ\}^{\alpha,\beta}(n-m)M^{2+}OZ \rightleftarrows m\{S^{2-}M^{2+}\}2m\{HOZ\}^{\alpha,\beta}(n-m)M^{2+}OZ \rightleftarrows m\{MS\}_{o,i}2m\{HOZ\}^{\alpha,\beta}(n-m)M^{2+}OZ$$

The first point to note here is that the virgin $M^{2+}OZ$ will contain some divalent extraframework cations that have participated in the water hydrolysis reaction described earlier.[8,11,14] Therefore, in the above reaction scheme involving multivalent cations, one must also take due cognizance of the following type of acid–base chemistry:

$$ZOM^{2+}OH^- + H_2S \rightleftarrows ZOM^{2+}SH^- + H_2O$$

This equilibrium is likely to lie to the right in view of the higher acidity of H_2S relative to H_2O, but nevertheless represents a point that needs to be studied in detail.

The second point concerns the fact that both metal hydrosulfides and metal sulfides will probably be involved in the formation of contact ion pairs and aggregated semiconductor clusters, existing in an intrazeolite Brønsted acidic microenvironment. The energetics and dynamics of these equilibria requires very careful experimental scrutiny. A third point relates to the larger size and lower acidity of HS^- relative to HBr (an isoelectronic pair) in the above kinds of intrazeolitic equilibria. Because of the spacial constraints on the passage of these species through the 2.3-Å diameter window of an oxygen six-ring, it is interesting that the

(20) Dwyer, I.; Dyer, A. *Chem. Ind.* **1984**, 237, and references therein.

reported $[Cd(S,O)]_4ZY$ cluster has been shown to exist in the β-cage of the zeolite rather than the α-cage with no sign of cadmium hydrosulfide clusters.[4] It is likely that the involvement of divalent cations and the use of high-temperature reaction conditions are responsible for β-cage rather than α-cage housing of cadmium sulfide clusters.[4] Clearly many important questions still need to be addressed if one is to begin to be able to routinely create monodispersed intrazeolite quantum crystallites by design. These will form the subject of ongoing investigations in our laboratory.

Acknowledgment. We acknowledge the Natural Sciences and Engineering Research Council of Canada's Operating and Strategic Grants Programmes (G.A.O.) and Office of Naval Research (G.D.S.) for generous financial support of this work. Invaluable technical discussions with and supplies of high-quality zeolites from Dr. Edith Flanigen at Union Carbide, Tarrytown, NY, proved to be especially worthwhile. S.Ö. expresses his gratitude to the Middle East Technical University for granting him an extended leave of absence to conduct his research at the University of Toronto. The expert assistance of Andreas Stein with the HX/Na,OH-SOD experiments and Lisa McMurray (an NSERC Summer Scholar) with the $HX/M_{56}Y$ experiments is deeply appreciated. We also thank all of our co-workers at Toronto for many stimulating and enlightening discussions during the course of this work. Finally, Dr. Zelimir Gabelica is acknowledged for suggesting the name proton-loaded zeolites for the materials reported in this paper.

Passivation of Photocarrier Recombination on CdS Photoanode by Two-Color Excitation

Seiichiro Nakabayashi and Akira Kira*

The Institute of Physical and Chemical Research (RIKEN), Wako-Shi, Saitama 351-01, Japan
(Received: November 15, 1989; In Final Form: April 9, 1990)

A CdS single-crystal photoelectrode in aqueous solution containing sodium sulfite was subjected to two-color excitation. The photocurrent caused by UV excitation was markedly enhanced by simultaneous sub-bandgap excitation; no photocurrent occurred for the sub-bandgap excitation alone. The enhancement is explained in terms of passivation of a recombination center by sub-bandgap excitation. The presence of such a recombination center is supported by photocapacitance measurement. Polarized two-color excitation and electrolyte electroreflectance spectroscopy revealed that the recombination center is not localized on the uppermost surface layer but penetrates inside.

Introduction

Intervalence states including surface states are regarded as playing the role of a charge trap or a recombination center in electron transfer at semiconductor/electrolyte interfaces.[1-10] Passivation of the recombination center is important not only from the practical point of view that it improves the photovoltaic conversion efficiency but also from the more fundamental point of view that such a study may offer solid information on the mechanism of charge recombination on which rather speculative discussions have been made. The present study is concerned with passivation of the recombination center of a cadmium sulfide (CdS) photoelectrode in aqueous solution.

In previous papers,[11,12] we have reported a depth-resolved electron-capture cross section of deep intervalence states in the space charge layer of a ZnO electrode and some surface anomalies that affect the experiment, and pointed out the possibility that the anomalies could be removed by simultaneous two-color excitation of both intervalence state and interfering states. Two-color excitation can probably be applied generally to the study of the electron or hole transfer in which intervalence states are involved. The present study is the first demonstration of this idea for cadmium sulfide, where the reactivity of a charge recombination center of the crystal was controlled by the second excitation.

Experimental Section

Photocurrent action spectra were measured for the xenon lamp (150W) light monochromated by through a Jovan-Yvon H-20 monochromator with a wavelength scanner MIC11. The light was modulated at 87 Hz by using a Stanford Research SR540 light chopper. Photocurrents were measured by using a Toho-Giken 2020 potentiostat and a NF Circuit Block LI-575 lock-in amplifier and recorded on a Riken Denshi SPG3C recorder. The intensity spectrum of the monochromated light was measured by using YSI-Kettering Model-65A radiometer.

In two-color excitation experiments, the main (first) excitation was made by the UV (351 and 364 nm, 20 mW) beam of the argon ion laser (Lexel Model 95) modulated at 815 Hz and the second excitation by the monochromated light of the xenon lamp. Spectra were taken for the wavelength of the second excitation. For the second excitation with polarized light, the Glan-Thompson prism was inserted in the optical path from the xenon lamp.

Photocapacitance action spectra were measured by the lock-in method, by which both the phase angle and the amplitude of the photocurrent were measured for the sinusoidal potential perturbation with an amplitude of 10 mV at 1 kHz. A Hewlett-Packard 3314A function generator was connected to the potentiostat for modulation of the electrode potential. The irradiation wavelength was scanned from longer to shorter direction.

EER spectra were measured for the monochromated xenon lamp light. The electrode potential was modulated by square wave at 79 Hz by using the potentiostat connected with the function generator. Light reflection was detected by a Hamamatsu Photonics R-928 photomultiplier and the signal was fed into the lock-in

(1) Evenor, M.; Gottesfeld, S.; Harzion, Z.; Huppert, D.; Feldberg, S. W. *J. Phys. Chem.* **1984**, *88*, 6213.
(2) Evenor, M.; Huppert, D.; Gottesfeldt, S. *J. Electrochem. Soc.* **1986**, *133*, 296.
(3) Tufts, B. J.; Abrahams, I. L.; Casagrande, L. G.; Lewis, N. S. *J. Phys. Chem.* **1989**, *93*, 3260.
(4) Nagasbramanian, G.; Wheeler, B. L.; Hope, G. A.; Bard, A. J. *J. Electrochem. Soc.* **1983**, *130*, 385.
(5) Finlayson, M. F.; Wheeler, B. L.; Kakuta, N.; Park, K. H.; Bard, A. J.; Campion, A.; Fox, M. A.; Webber, S. E.; White, J. M. *J. Phys. Chem.* **1985**, *89*, 5676.
(6) Jakubowicz, A.; Mahalu, D.; Wolf, M.; Wold, A.; Tenne, R. *Phys. Rev. B* **1989**, *40*, 2992.
(7) Haneman, D.; McCann, J. F. *Phys. Rev. B* **1982**, *25*, 1241.
(8) Heller, A.; Leamy, H. J.; Miller, B.; Jhonston Jr, W. D. *J. Phys. Chem.* **1983**, *87*, 3239.
(9) Nelson, R. J.; Williams, J. S.; Leamy, H. J.; Miller, B.; Casey, H. C.; Parkinson, B. A.; Heller, A. *Appl. Phys. Lett.* **1980**, *36*, 76.
(10) Wilson, R. H. *J. Electrochem. Soc.* **1979**, *126*, 1187.
(11) Nakabayashi, S.; Kira, A.; Ipponmatu, M. *J. Phys. Chem.* **1989**, *93*, 5543.
(12) Nakabayashi, S.; Kira, A. *J. Phys. Chem.* **1987**, *91*, 374.

0022-3654/90/2094-7571$02.50/0